International Journal of Nanomedicine

Dovepress
open access to scientific and medical research

Open Access Full Text Article

ORIGINAL RESEARCH

Bacteria-Targeting Nanoparticles with ROS-Responsive Antibiotic Release to Eradicate Biofilms and Drug-Resistant Bacteria in Endophthalmitis

Jian Yu[1,2,*], Huan Xu[1,2,*], Jiaojiao Wei[1,2], Liangliang Niu[1,2], Haohao Zhu[1,3], Chunhui Jiang[1,2]

[1]Department of Ophthalmology and Visual Science, Eye, Ear, Nose and Throat Hospital, Shanghai Medical College of Fudan University, Shanghai, People's Republic of China; [2]Key Laboratory of Myopia of State Health Ministry and Key Laboratory of Visual Impairment and Restoration of Shanghai, Shanghai, People's Republic of China; [3]Department of Ophthalmology, Shanghai Fifth People's Hospital, Fudan University, Shanghai, People's Republic of China

*These authors contributed equally to this work

Correspondence: Chunhui Jiang, Department of Ophthalmology and Vision Science, Eye and ENT Hospital, Fudan University, 83 Fenyang Road, Shanghai, 200031, People's Republic of China, Email chhjiang70@163.com; Haohao Zhu, Department of Ophthalmology, Shanghai Fifth People's Hospital, Fudan University, 128 Ruili Road, Shanghai, 200240, People's Republic of China, Tel +86-21-64308151, Fax +86-21-64300477, Email haohao700315@163.com

Background: Bacterial endophthalmitis is an acute progressive visual threatening disease and one of the most important causes of blindness worldwide. Current treatments are unsatisfactory due to the emergence of drug-resistant bacteria and the formation of biofilm.

Purpose: The aim of our research was to construct a novel nano-delivery system with better antimicrobial and antibiofilm effects.

Methods: This study developed a novel antibiotic nanoparticle delivery system (MXF@UiO-UBI-PEGTK), which is composed of (i) moxifloxacin (MXF)-loaded UiO-66 nanoparticle as the core, (ii) bacteria-targeting peptide ubiquicidin (UBI_{29-41}) immobilized on UiO-66, and (iii) ROS-responsive poly (ethylene glycol)-thioketal (PEG-TK) as the surface shell. Then the important properties of the newly developed delivery system, including biocompatibility, toxicity, release percentage, thermal stability, ability of targeting bacteria, and synergistic antibacterial effects on bacterial biofilms and endophthalmitis, were evaluated.

Results: In vitro, MXF@UiO-UBI-PEGTK exhibited significant antibiotic effects including the excellent antibiofilm property against *Staphylococcus aureus, Pseudomonas aeruginosa*, and methicillin-resistant *Staphylococcus aureus* at high levels of ROS. Moreover, MXF@UiO-UBI-PEGTK demonstrated outstanding efficacy in treating bacterial endophthalmitis in vivo.

Conclusion: This novel nanoparticle delivery system with ROS-responsive and bacteria-targeted properties promotes the precise and effective release of drugs and has significant potential for clinical application of treating bacterial endophthalmitis.

Keywords: endophthalmitis, nanoparticles, bacterial biofilms, ROS-responsive, moxifloxacin

Introduction

Endophthalmitis, which is a severe inflammation of intraocular fluids (vitreous and aqueous) and tissues, generally leads to total loss of vision or atrophy of the eyeball. The most prevalent causes of endophthalmitis are intraocular surgery, trauma, and endogenous infection.[1] Furthermore, the most common microorganism that causes such inflammation is bacteria.[2] Currently, bacterial endophthalmitis is generally treated with an intravitreal injection of antibiotics with or without vitrectomy.[3] Despite these efforts and the development of new antibiotics, most patients with bacterial endophthalmitis have a very poor visual prognosis (20/400 or worse).[2] The main reasons for these unfavorable results include the formation of biofilms and the emergence of drug-resistant bacteria.[4,5]

Received: 11 August 2023
Accepted: 10 March 2024
Published: 20 March 2024

Graphical Abstract

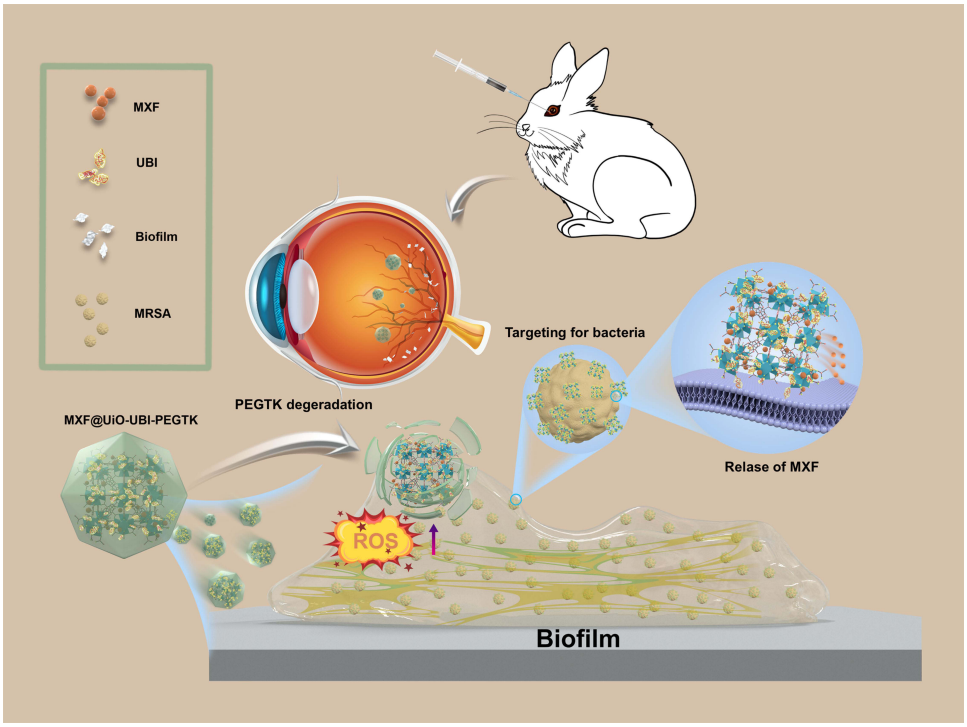

Bacterial biofilms are a type of membrane formed by bacteria and constitute encysted complexes secreted by bacteria after adsorption onto active or inactive surfaces, including polysaccharide matrix, fibronectin, lipoprotein, and other polysaccharide proteins.[6] By decreasing the permeability of antibiotics, bacterial biofilms significantly increase the pathogenicity and drug resistance of bacteria.[7] To address the issue of biofilm formation, several strategies have been applied, including chemotherapy, such as those using new antibiotics, and non-chemotherapy, such as those involving targeted antibacterial systems.[8–10] Ideal intravitreal antibiotics should exhibit low toxicity and broad-spectrum antibacterial properties. Moxifloxacin (MXF) is a fourth-generation quinolone that inhibits deoxyribonucleic acid (DNA) gyrase and topoisomerase in microorganisms and exhibits satisfactory antibacterial activity against both gram-positive (*Staphylococcus aureus* (*S. aureus*)) and gram-negative bacteria (*Escherichia coli*, (*E. coli*)).[11] A previous study showed that MXF has the advantage of minimal toxicity compared to vancomycin and cefuroxime.[12]

In addition, various attempts have been made to develop targeted antibacterial systems, and nanoparticles (NPs) are promising candidates.[13–15] NPs can efficiently load antibiotics. Furthermore, various targeting materials can be added or immobilized into it. Metal-organic framework (MOF), one of the NPs, which are a class of porous crystalline materials formed by the self-assembly of metal ions with one or more multifunctional organic ligands via coordination interactions.[16] The diverse ligand structures of MOFs provides them flexible structures with excellent properties, including large specific surface areas, adjustable pore sizes, and good thermal stability.[17,18] These characteristics render MOFs suitable candidates for biomedical applications.[19] UiO-66 is a typical MOF composed of $[Zr_6O_4(OH)_4]$ octahedron clusters linked with 1,4-benzene dicarboxylic acid ligands and exhibits low toxicity, porosity, and good biocompatibility.[20] In this study, we synthesized UiO-66 as a carrier for MXF loading.

There are several strategies to achieve the targeting effect, one of which is using the microenvironment-responsive method, such as pH-sensitive,[21–23] temperature-sensitive,[24] enzyme-sensitive,[25] and light-sensitive[26,27] methods. In inflammatory tissues, reactive oxygen species (ROS) is 10 times higher than that in the normal tissues.[28] Therefore, the difference in ROS levels between normal and inflammatory tissues provides a potential advantage in creating an

ROS-sensitive delivery system with site-specific drug release properties. Researchers have applied ROS-responsive NP-based drug delivery systems in the targeted therapy of several diseases, including cancer, osteoarthritis, thrombosis, and wound healing.[14,29–32] However, few studies have focused on its application in ophthalmic medicine. Polyethylene glycol-thioketal (PEG-TK) is a typical ROS-responsive compound. In particular, the thioketal (TK bond) is one of the most effective ROS-responsive moieties because of its stability under biological conditions as well as its rapid decomposition into acetone and thiol moieties triggered by high levels of ROS.[33,34] Li et al reported that PEG-TK can increase antibacterial efficacy by controlling the release of vancomycin.[35] Although the ROS-responsive delivery system can increase the local concentration of antibiotics in the infectious area, it lacks target specificity to the bacteria and biofilms.

Ubiquicidin (UBI_{29-41}), which is a cationic human antimicrobial peptide fragment with six positively charged residues, showed high specificity and target accuracy for bacterial infection owing to the interaction between the cationic domain of UBI_{29-41} with positive charge and the bacterial surface with negative charge.[36] This property renders UBI_{29-41} an ideal bacteria-targeting ligand.

To address the challenge of biofilm formation, UiO-66 was used to absorb MXF, followed by the immobilization of UBI_{29-41}. Subsequently, we introduced PEG-TK to modify the surface of the NPs to construct an ROS-sensitive drug delivery system–the final complex NPs (MXF@UiO-UBI-PEGTK) (Scheme 1). When the NPs were injected into the vitreous cavity, PEG-TK outside the NPs degraded rapidly around the inflammation area with a high level of ROS. Next, the UBI_{29-41} groups actively guided the NPs to the area wherein the bacteria were aggregated, such as a biofilm. We hypothesized that this ROS-sensitive, bacterial-targeted MXF delivery system might achieve the goal of "1 + 1 > 2". In this study, important properties of the newly developed delivery system, including biocompatibility, toxicity, release percentage, thermal stability, targeting ability, and synergistic antibacterial effects on bacterial biofilms and endophthalmitis, were evaluated.

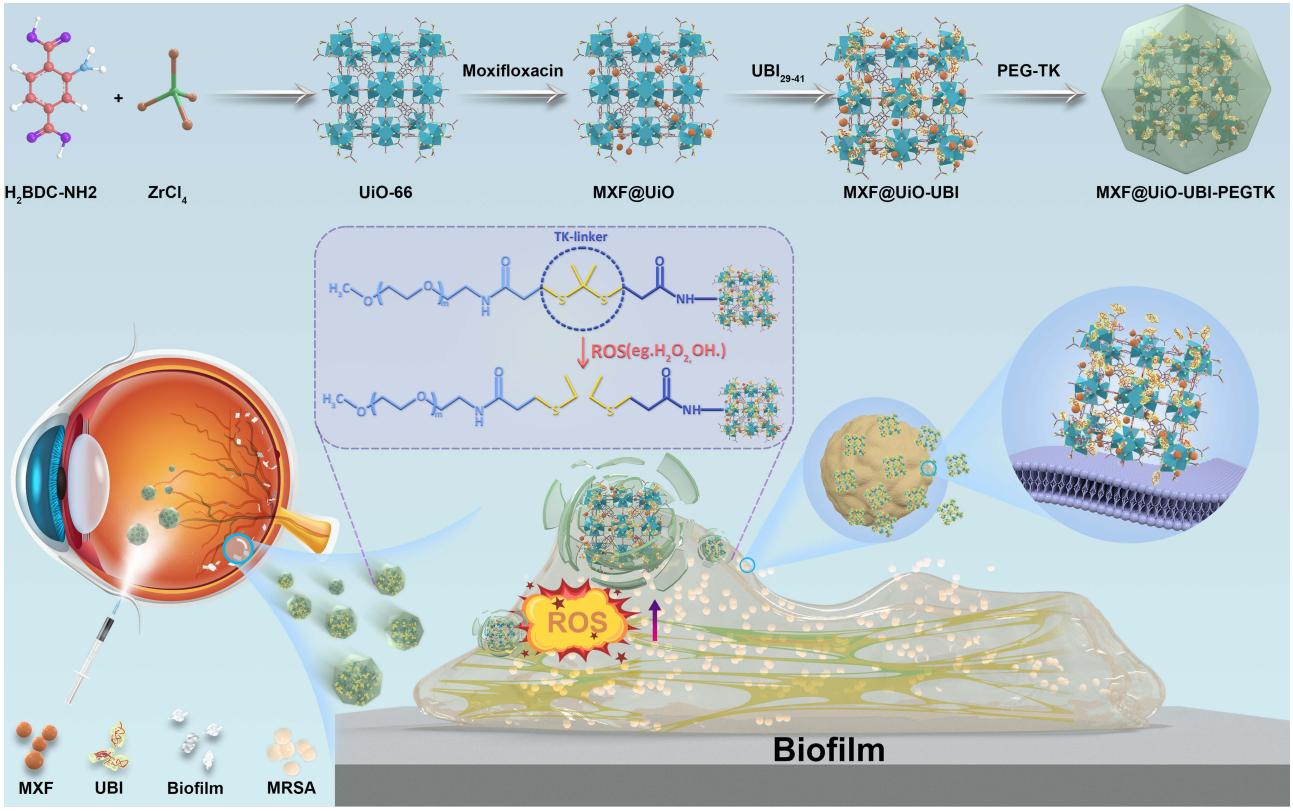

Scheme 1 Schematic illustration of the construction of MXF@UiO-UBI-PEGTK system and its therapeutic mechanisms in endophthalmitis.

Materials and Methods

Synthesis of UiO-66

First, 90 mg of amino terephthalic acid, 115 mg of zirconium chloride, 1.8 g of benzoic acid, and 80 μL of concentrated hydrochloric acid were added into 35 mL of dimethylformamide (DMF) and stirred until fully dissolved and then placed in a hydrothermal kettle at 120 °C for 10 h. After the kettle was completely cooled, the mixture was centrifuged at 15,000 rpm for 30 min and washed three times with ethanol. Finally, the obtained material was soaked in an ethanol solution for three days to remove the unreacted organic solvent. The materials were centrifuged and freeze-dried before further use.

Adsorption of MXF

MXF (100 mg) and UiO-66 (50 mg) were dispersed in 200 mL of ethanol and stirred for 24 h. Subsequently, the resulting solution was centrifuged, freeze-dried, and reserved for further use.

Introduction of the UBI_{29-41} Target

First, the carboxyl group of UBI_{29-41} was activated by adding UBI_{29-41} (1 mg/mL, dissolved in deionized water) to ethylcarbodiimide hydrochloride (EDC) (pH 5.6, 5 mg/mL) and stirring the solution for 2 h at 37 °C. Next, an equal volume of 2 mg/mL of UiO-66 adsorbed with MXF was added, and later, 5 mg/mL of N-hydroxysuccinimide (NHS) solution was added and stirred at 25°C for 24 h to attach the amino group of UiO-66 with the carboxyl group of UBI_{29-41}. Thereafter, the material was freeze-dried for further use.

Preparation of PEGTK Layers

First, the carboxyl group of PEG-TK was activated by adding PEG-TK (1 mg/mL, dissolved in deionized water) to ethylcarbodiimide hydrochloride (EDC) (pH 5.6, 5 mg/mL) and stirring the solution for 2 h at 37 °C. Next, an equal volume of 2 mg/mL of MXF@UiO-UBI was added, and later, 5 mg/mL of N-hydroxysuccinimide (NHS) solution was added and stirred at 25°C for 24 h to attach the amino group of MXF@UiO-UBI with the carboxyl group of UBI_{29-41}. Thereafter, the material was freeze-dried for further use.

Characterization of Nanoparticles

The ultrastructure of UiO-66, MXF@UiO, and MXF@UiO-UBI-PEGTK was examined by transmission electron microscopy (TEM). The nanoparticles were dissolved in ethanol to a concentration of 5 mg/mL, and 5 μL of the solution was aspirated and transferred to a carbon-coated copper TEM grid. After air-drying, the samples were imaged using the high-resolution TEM (JEOL JEM2100F, Tokyo, Japan). The diameter of the NPs (UiO-66, MXF@UiO, and MXF@UiO-UBI-PEGTK) dissolved in potassium phosphate buffer and 10% diluted fetal bovine serum was determined using the dynamic light scattering (DLS) method (Brookhaven Instrument, USA, BI-200SM). TGA was carried out with an STA 6000 simultaneous thermal analyzer (PerkinElmer, Waltham, MA, USA) from 30 to 850 °C to check the thermal stability in air.

To obtain the release profiles of MXF from MXF@UiO-UBI-PEGTK, MXF@UiO-UBI-PEGTK (50 μg/mL) immersed in PBS (2 mL) without or with different concentrations of H_2O_2 (0.01 mM, 0.25 mM, 1.0 mM) with an optical density (OD) at 600 nm of 1.0 was introduced into the centrifuge tube at 37 °C. At predetermined time points, 300 μL of the solution was purified using an Amicon Ultra-0.5 mL centrifugal filter (Millipore, Billerica, MA, USA). The MXF concentration in the filtrate was determined by measuring the maximum ultraviolet-visible (UV-vis) light absorbance of MXF at $\lambda = 288$ nm using a Multimode Reader equipped with a UV-vis detector (Infinite 200 PRO; TECAN, Mä nnedorf, Switzerland).

Similarly, the drug loading and encapsulation rate were determined using the UV-vis detector at 288 nm. The amount of encapsulated drug was calculated from the absorbance of the supernatant of the unencapsulated drug using the following equation.

$$\text{Encapsulation rate} = \frac{\text{weight of moxifloxacin in nanoparticles}}{\text{weight of moxifloxacin used}}$$

$$\text{Drug loading rate} = \frac{\text{weight of moxifloxacin in nanoparticles}}{\text{total weight of moxifloxacin and excipients}}$$

Cellular Compatibility of MXF, UiO-66, and MXF@UiO-UBI-PEGTK

Retinal pigment epithelium cells (RPEs) and retinal microvascular endothelial cells (RMECs) were seeded in mixed Dulbecco's modified Eagle's medium (DMEM) supplemented with 10% fetal bovine serum, 100 U mL^{-1} penicillin, and 100 μg mL^{-1} streptomycin in a 5% CO_2 incubator at 37 °C. After incubation with different concentrations of MXF, UiO-66, and MXF@UiO-UBI-PEGTK, the medium of RPEs and RMECs was replaced with a new medium (100 μL) containing CCK-8 (10 μL, Beyotime, China). Water-soluble formazan was formed after 2 h incubation at 37 °C, which was aspirated to a new 96-well plate for absorbance measurement using microplate reader (Spark, TECAN) at 450 nm. To assess live and dead cells, RPEs and RMECs treated by MXF, UiO-66, or MXF@UiO-UBI-PEGTK were detected with a live/dead assay using calcein-AM and propidium iodide (PI) (catalog # C-3099 and P-3566, Invitrogen, Carlsbad, CA, USA). Both stains (100 μL, 5% calcein-AM, and 10% PI in DMEM) were applied to each well of confocal glass-bottom 96-well plates. Calcein-AM was hydrolyzed by an esterase in live cells with intact cell membranes to form fluorescent calcein, whereas PI stained the cells with compromised cell membranes. Approximately 40 min after staining, the cells were examined using Confocal laser scanning microscopy (CLSM).

Determination of MIC and MBC

To measure the minimum inhibitory concentration (MIC) and minimum bactericidal concentration (MBC), *S. aureus*, methicillin-resistant *S. aureus* (MRSA), and *Pseudomonas aeruginosa* (*P. aeruginosa*) were cultured using the broth microdilution method. MXF, UiO-66, or MXF@UiO-UBI-PEGTK (100 μL) was prepared in Mueller-Hinton broth (MHB). MXF and MXF@UiO-UBI-PEGTK were added at different MXF equivalent concentrations (0–64 μg/mL), while the UiO-66 concentration was the same with that used for MXF@UiO-UBI-PEGTK. Subsequently, 100 μL of *S. aureus, P. aeruginosa*, or MRSA (1×10^6 cells mL^{-1}) in MHB with or without 0.5 mM H_2O_2 was added to each well. The microplate was incubated for 24 h at 37 °C. The MIC values were obtained at the lowest concentrations at which no bacterial growth was visible to the naked eye. Thereafter, 10 μL of each clear suspension was plated onto blood agar. The plates were incubated at 37 °C for 24 h. MBC values were obtained at the lowest concentration at which no visible growth was observed on the agar plates. After exposure to MXF or MXF@UiO-UBI-PEGTK, the growth inhibition curve of the bacteria was evaluated (OD=600 nm) using a microplate reader (Spark, TECAN) every 2 h for 24 h. The experiments were repeated three times.

Evaluation of Targeting Effect

The bacterial affinity of MXF@UiO and MXF@UiO-UBI-PEGTK for three kinds of bacteria was investigated by SEM. 24-h-old *S. aureus*, MRSA and *P. aeruginosa* biofilms in 48-well plates were treated with MXF@UiO and MXF@UiO-UBI-PEGTK at MXF (equivalent) concentrations of 2 mg mL^{-1} for 1 h. After exposure, biofilms were scrapped from the bottom of the well and subsequently subjected to centrifugation at a speed ranging from 3000 to 4000 rpm. The supernatant was then discarded, and the samples were washed three times with 1X PBS at a pH of 7.2–7.4. During the washing process, the cells were gently resuspended, followed by another round of centrifugation and removal of the supernatant. The biofilms were then fixed with a 2.5% glutaraldehyde solution for a duration of 2 hours. Subsequently, the biofilms were sequentially dehydrated using solutions of 30%, 50%, 70%, 90%, 95%, and 100% ethanol (v/v in water), as well as 50% ethanol in acetone, each for a period of 10 minutes. Finally, the biofilms were dehydrated twice with pure acetone for 15 minutes each time. After air-drying, the samples were imaged at an accelerating voltage of 15 kV.

Exposure of Biofilm to Antimicrobials

For biofilm penetration assessment, S. aureus and MRSA were cultured in confocal glass-bottom 96-well plates under static conditions at 37°C for 24 hours. The culture medium consisted of Tryptic Soy Broth (TSB) supplemented with 2% glucose to facilitate biofilm formation. After biofilm formation, the culture medium was aspirated, and the biofilms were washed three times using sterile water to eliminate planktonic cells and residual media. Subsequently, 24-h-old *S. aureus* and MRSA biofilms in confocal glass-bottom 96-well plates were exposed to MXF and MXF@UiO-UBI-PEGTK at MXF (equivalent) concentrations of 1 μg mL^{-1} for 6 h with or without 0.25 mM H_2O_2. After exposure, the culture medium was aspirated, and the biofilms underwent three washes with sterile water to eliminate planktonic cells and residual media. The biofilms were stained in the dark for 15 minutes with the LIVE/DEAD BacLight bacterial viability kit (L-7012, Invitrogen). Subsequently, the confocal glass-bottom 96-well plates were promptly subjected to imaging using CLSM, and three-dimensional (3D)-CLSM images were obtained.

To assess the eradication of bacterial biofilms, 24-h-old *S. aureus*, MRSA, and *P. aeruginosa* biofilms in 96-well plates were exposed to MXF and MXF@UiO-UBI-PEGTK at MXF (equivalent) concentrations of 10 and 50 μg mL^{-1} for 24 h with or without 0.25 mM H_2O_2. After exposure, the culture medium was aspirated, and the biofilms underwent three washes with sterile water to eliminate planktonic cells and residual media. The biofilms were stained with a LIVE/DEAD BacLight bacterial viability kit (L-7012, Invitrogen) for 15 min in the dark before they were imaged using CLSM as described in detail above. Furthermore, in a separate experiment, after exposure to the antimicrobials as described above, biofilms were resuspended by scraping from the bottom of the well, after which a plastic sterile sticker was placed over the plate, and the plate was washed for 8 min to further disperse the biofilm. Next, the suspension was serially diluted in PBS, and 100 μL of each dilution was spread onto plate count agar plates and incubated at 37 °C for 24 h. Finally, the number of colony forming units (CFUs) was counted and expressed as CFU cm^{-2}.

For validating the eradication of bacterial biofilms using SEM, S. aureus, MRSA, and P. aeruginosa were cultured on gelatin-coated cell coverslips within 6-well plates to cultivate 24-hour-old biofilms. Subsequently, the biofilms were exposed to MXF and MXF@UiO-UBI-PEGTK at MXF (equivalent) concentrations of 50 μg mL^{-1} for 24 h with or without 0.25 mM H_2O_2. After exposure, the culture medium was aspirated, and the biofilms were washed three times using sterile water to eliminate planktonic cells and residual media fixed with a 2.5% glutaraldehyde solution for 2 h. With 30, 50, 70, 90, 95, and 100% (v/v, in water), and 50% ethanol in acetone for 10 min each time, and finally dehydrated them twice with pure acetone for 15 min. After air-drying. the samples were imaged at an accelerating voltage of 15 kV using SEM.

In vivo Antibacterial Tests

For the in vivo antibacterial property evaluation, New Zealand white rabbits (3 months old, weighing 2.0–2.5 kg) were purchased from Slaccas Co. (Shanghai, China) and used to establish the bacterial endophthalmitis model before drug intervention. All experimental procedures in the study were approved by the Animal Ethics Committee of the Eye and Ear Nose Throat Hospital of Fudan University and complied with Association for Research in Vision and followed National Institutes of Health guide for the care and use of Laboratory animals. Rabbits were evenly separated into three groups and treated with PBS, MXF, or MXF@UiO-UBI-PEGTK. The suspension was prepared with serial dilutions to achieve a concentration of 10^4 CFUs mL^{-1}. After the pupil of the rabbit was dilated, and the rabbit was administered general and topical anesthesia, anterior chamber paracentesis was performed to avoid excessive intraocular pressure. Using an operating microscope (Zeiss, Oberkochen, Germany), 100 μL of *S. aureus, P. aeruginosa*, or MRSA suspension was slowly injected into the vitreous cavity (mid-vitreous) via the pars plana, 2 mm posterior to the temporal bulbar limbus, using a 30-gauge needle, 1 mL tuberculin syringe, with the bevel of the needle facing the lens to keep it away from it. On the second day, the formation of endophthalmitis was observed using a slit-lamp and indirect ophthalmoscopy.

After the successful construction of the bacterial endophthalmitis model, 0.1 mL of PBS, MXF, or MXF@UiO-UBI-PEGTK (500 μg mL^{-1} MXF (equivalent)) was injected into the vitreous cavity. Changes in the anterior segment of the eye were observed using slit lamps and indirect ophthalmoscopes at 1, 3, 7, and 10 d, respectively. After taking pictures

on the 10th day, approximately 0.1 mL of vitreous fluid was aspirated from the eyes. Next, the suspension was serially diluted in PBS, and 100 μL of each dilution was spread onto plate count agar plates and incubated at 37 °C for 24 h. Finally, the number of CFUs was counted and expressed as CFU cm^{-2}. The animals were sacrificed, and the eyeballs were removed. The eyeballs were placed in a fixative solution for at least 24 h. After embedding in paraffin, the eyeballs were cut into tissue sections (thickness: 5 mm). The tissues were then mounted onto slides for H&E staining. Images were obtained using an optical microscope. For estimating the inflammation score of bacterial infections after different treatments, the clinical inflammation degree score was calculated according to the Peyman's method. A slit lamp and ophthalmoscope were used to observe the ocular inflammation reaction at 0, 1, 3, 7, and 10 d after modeling.

Results and Discussion

Characterization of MXF@UiO-UBI-PEGTK

TEM was used to visualize the morphologies of UiO-66, MXF@UiO, and MXF@UiO-UBI-PEGTK. The results confirmed that all NPs were spherical and homogeneous (Figure 1A). The elemental mapping and the quantitative elemental compositions spectrum of UiO-66 was derived using the TEM-energy dispersive spectroscopy and SEM-energy dispersive spectroscopy elemental analysis (Figure 1B and C). Dynamic light scattering (DLS) measurements showed that UiO-66, MXF@UiO, and MXF@UiO-UBI-PEGTK had mean diameters of 78, 100, and 115 nm, respectively (Figure 1D). Thermal stability was investigated using thermogravimetric analysis (TGA). The decomposition of MXF with a gradual loss of weight was initially observed between 36 and 98 °C, and a secondary weight loss occurred at 231 °C. With further increase in temperature, MXF decomposed completely. Compared to MXF, MXF@UiO-UBI-PEGTK was more thermally stable and showed a weight loss plateau up to 850 °C, where only 40% of its original weight was lost (Figure 1E). The drug loading and entrapment efficiency of UiO-66 for moxifloxacin is 39% and 59%. Based on the chemical molecular structure of moxifloxacin as well as UiO-66, it is hypothesized that the driving force for loading is the hydrogen-bonding and ionic bonds between the secondary and tertiary amine groups in moxifloxacin and the carboxyl of UiO-66. Additionally, previous studies suggest that π-π interactions between the aromatic rings of the drug and the MOF material facilitate the physical adsorption of the drug.[37,38]

Release of MXF and Detection of ROS Generation

The MXF release behavior of MXF@UiO-UBI-PEGTK was investigated. The release of MXF from MXF@UiO-UBI-PEGTK in phosphate buffer solution (PBS) was 17% at 24 h. Furthermore, this release increased to 25%, 50%, and 85% with 0.01, 0.25, and 1 mM of H_2O_2 at 24 h, respectively (Figure 1F). This result suggests that the release of MFX from MXF@UiO-UBI-PEGTK was relatively stable under physiological conditions, and H_2O_2 significantly promoted the release of MXF. The TK bond is ROS-cleavable, and easier to decompose in a microenvironment with high degrees of ROS-like inflammation. The more rapid degradation of MXF@UiO-UBI-PEGTK and the increase in the release of MXF with an increase in the H_2O_2 concentration could be potential advantages in the clinical setting.

ROS generation was detected using the fluorescent probe-Dichlorodihydrofluorescein diacetate (DCFH-DA) in RPEs and RMECs (Figure S1). The intensity of fluorescence in cells represents the level of ROS. Fluorescence intensity was very weak in PBS-treated RPEs and RMECs. When treated with lipopolysaccharides (LPS), the fluorescence intensity increased significantly in an LPS concentration-dependent manner. This result is consistent with other reports, confirming that inflammation could induce a microenvironment of excessive ROS in tissues and cells.[39–41]

Evaluation of Cellular Biocompatibility

The biocompatibility of MXF@UiO-UBI-PEGTK was explored by evaluating the relative cell viability using a cell counting kit and apoptosis detection using a fluorescent staining method and flow cytometric analysis. The relative cell viability of RMECs and RPEs significantly decreased when the MXF concentration was increased to 100 and 350 μg/mL, respectively. MXF@UiO-UBI-PEGTK started to inhibit the viability of RMECs and RPEs when the MXF equivalent concentration reached 350 and 500 μg/mL, respectively (Figure 2A and B). The fluorescence images of live/dead cell staining showed that the number of live RMECs and RPEs decreased when the MXF concentration was increased to 100

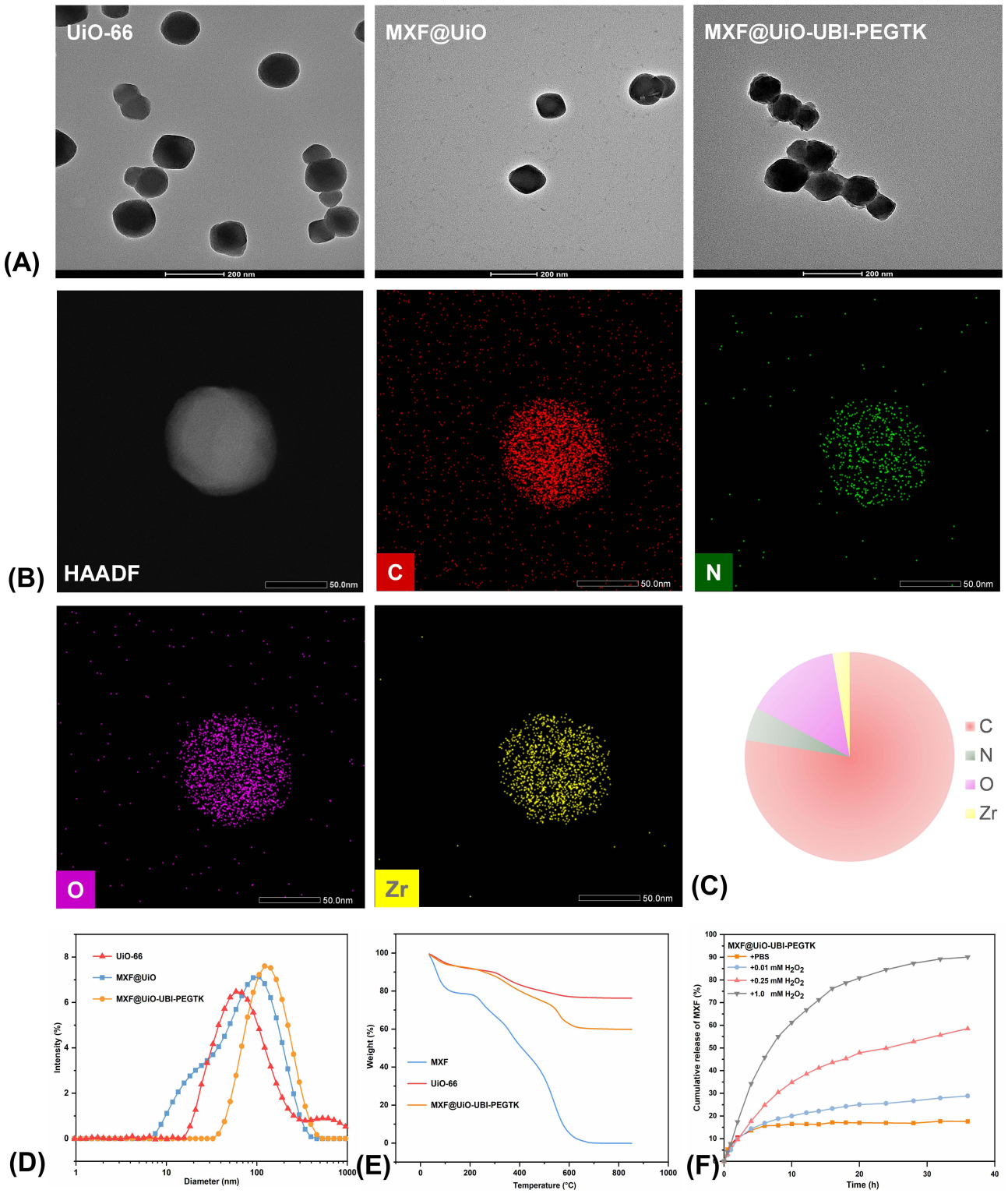

Figure 1 Structural and physio-chemical characterization of MXF@UiO-UBI-PEGTK. (**A**) TEM images of UiO-66, MXF@UiO, and MXF@UiO-UBI-PEGTK. Scale bar: 200 nm. (**B**) A corresponding High-Angle Annular Dark Field (HAADF) micrograph and TEM-EDS elemental mapping of UiO-66. Scale bar: 50 nm. (**C**) Element compositions of UiO-66 calculated from their corresponding SEM-EDS spectra. (**D**) Corresponding diameter distribution curve. (**E**) TGA curves of UiO-66, MXF and MXF@UiO-UBI-PEGTK. (**F**) MXF release from MXF@UiO-UBI-PEGTK with different concentrations of H_2O_2 at different time points.

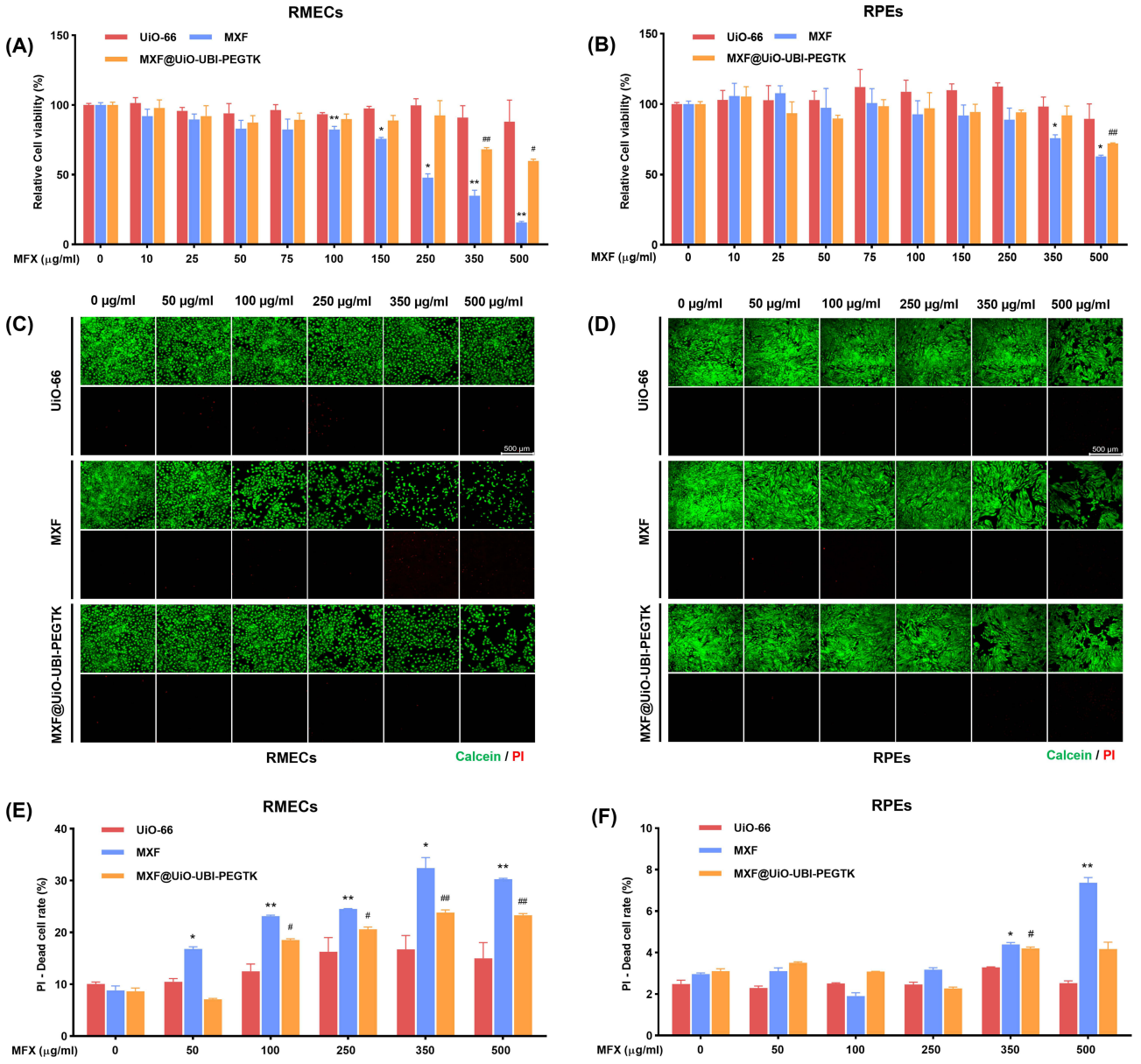

Figure 2 Evaluation of cellular biocompatibility of UiO-66, MXF, and MXF@UiO-UBI-PEGTK for RMECs and RPEs. Relative cell viability of (**A**) RMECs and (**B**) RPEs incubated with UiO-66, MXF, and MXF@UiO-UBI-PEGTK for 24 h (*p, $^{\#}p$ < 0.05; **p, $^{\#\#}p$ < 0.01) (*p, MXF vs UiO-66; $^{\#}p$, MXF@UiO-UBI-PEGTK vs UiO-66). Fluorescence images of live/dead staining on (**C**) RMECs and (**D**) RPEs after the incubation with UiO-66, MXF, and MXF@UiO-UBI-PEGTK for 24 h. Scale bar: 500 μm. The apoptosis rate of (**E**) RMECs and (**F**) RPEs incubated with UiO-66, MXF, and MXF@UiO-UBI-PEGTK for 24 h (*p, $^{\#}p$ < 0.05; **p, $^{\#\#}p$ < 0.01) (*p, MXF vs UiO-66; $^{\#}p$, MXF@UiO-UBI-PEGTK vs UiO-66).

and 350 μg/mL, respectively. After treatment with MXF@UiO-UBI-PEGTK, the number of these two types of live cells started to decrease when the MXF equivalent concentration was higher than 350 and 500 μg/mL, respectively (Figure 2C and D). Flow cytometric analysis showed that the dead cell rates of RMECs and RPEs significantly increased when the MXF concentration was increased to 50 and 350 μg/mL, respectively. After the administration of MXF@UiO-UBI-PEGTK, the dead cell rate of RMECs and RPEs started to increase when the MXF equivalent concentration reached 100 and 350 μg/mL, respectively (Figure 2E and F). These results indicated that MXF@UiO-UBI-PEGTK was less toxic to retinal cells than free MXF, even when a high dosage was used.

A high dosage of antibiotics has been considered an option in the treatment of endophthalmitis. However, it was reported that high doses of antibiotics, including MXF, can cause retinal toxicity.[42] In our study, a high dose of

MXF@UiO-UBI-PEGTK still showed excellent cellular biocompatibility, which could reduce the potential retinal tissue damage in clinical applications.

In vitro Antibacterial Test

The MIC and MBC of MXF@UiO-UBI-PEGTK were determined. Gram-positive (*S. aureus*), gram-negative (*P. aeruginosa*), and drug-resistant bacteria (MRSA) were selected for testing. The MIC and MBC of blank UiO-66 were higher than 64 μg/mL for all bacteria. The MIC and MBC of MXF were 0.25 and 1 μg/mL for *S. aureus*, 0.125 and 0.5 μg/mL for MRSA, and 1 and 4 μg/mL for *P. aeruginosa*, respectively. The addition of H_2O_2 (0.01 and 0.25 mM) did not affect the MIC and MBC of MXF. The MIC and MBC of MXF@UiO-UBI-PEGTK (at the same MXF equivalent concentration) were 0.25 and 1 μg/mL for *S. aureus*, 0.125 and 0.5 μg/mL for MRSA, and 2 and 8 μg/mL for *P. aeruginosa*, respectively. The addition of 0.25 mM H_2O_2 significantly decreased the MIC and MBC of MXF@UiO-UBI-PEGTK for *S. aureus* (0.0156 and 0.025 μg/mL, respectively) and MRSA (0.0315 and 0.025 μg/mL, respectively) (Tables 1–3). MXF@UiO-UBI-PEGTK inhibited the growth of three types of bacteria in an ROS-dependent manner (Figure S2). The above results show that the addition of H_2O_2 did not change the antibacterial effect of MXF. However, it enhanced the antibacterial and bacterial inhibitory efficiency of MXF@UiO-UBI-PEGTK. These results were attributed to the ROS-dependent MXF release from MXF@UiO-UBI-PEGTK.

Table 1 Minimum Inhibitory Concentration (MIC) and Minimal Bactericidal Concentration (MBC) of MXF, UiO-66 and MXF@UiO-UBI-PEGTK Against *S. Aureus* with Different Concentration of H_2O_2

Staphylococcus aureus	H_2O_2 0 mM		H_2O_2 0.01 mM		H_2O_2 0.25 mM	
	MIC	MBC	MIC	MBC	MIC	MBC
UiO-66	>64	>64	>64	>64	>64	>64
MXF	0.25	1	0.25	1	0.25	1
MXF@UiO-UBI-PEGTK	0.25	1	0.25	1	0.0156*	0.025*

Note: Unit: μg mL^{-1}. (*$p < 0.05$, MXF vs MXF@UiO-UBI-PEGTK)

Table 2 Minimum Inhibitory Concentration (MIC) and Minimal Bactericidal Concentration (MBC) of MXF, UiO-66 and MXF@UiO-UBI-PEGTK Against MRSA with Different Concentration of H_2O_2

MRSA	H_2O_2 0 mM		H_2O_2 0.01 mM		H_2O_2 0.25 mM	
	MIC	MBC	MIC	MBC	MIC	MBC
UiO-66	>64	>64	>64	>64	>64	>64
MXF	0.125	0.5	0.125	0.5	0.125	0.5
MXF@UiO-UBI-PEGTK	0.125	0.5	0.125	0.5	0.03125*	0.025*

Note: Unit: μg mL^{-1}. (*$p < 0.05$, MXF vs MXF@UiO-UBI-PEGTK)

Table 3 Minimum Inhibitory Concentration (MIC) and Minimal Bactericidal Concentration (MBC) of MXF, UiO-66 and MXF@UiO-UBI-PEGTK Against *P. Aeruginosa* with Different Concentration of H_2O_2

Pseudomonas aeruginosa	H_2O_2 0 mM		H_2O_2 0.01 mM		H_2O_2 0.25 mM	
	MIC	MBC	MIC	MBC	MIC	MBC
UiO-66	>64	>64	>64	>64	>64	>64
MXF	1	4	1	4	1	4
MXF@UiO-UBI-PEGTK	2	8	2	8	2	8

Note: Unit: μg mL^{-1}.

Targeting Effect Toward Bacteria

The target specificity of MXF@UiO-UBI-PEGTK against three types of bacteria (*S. aureus*, MRSA, and *P. aeruginosa*) was investigated using scanning electron microscopy (SEM). MXF-UiO was used as a control without modification with UBI_{29-41} and PEGTK. The SEM results showed that only a small number of MXF-UiO NPs were in contact with these three types of bacteria. After modification with UBI_{29-41} and PEGTK, the number of NPs combined with bacteria increased significantly. MXF@UiO-UBI-PEGTK was wrapped around the surface of bacteria and incorporated into the bacterial membrane (Figure 3). Additionally, in the former results, MXF@UiO-UBI-PEGTK showed a superior antibiotic effect over MXF. These indicate that UBI_{29-41} plays a synergistic role through target binding to bacteria with high specificity and affinity. This is consistent with the results of previous studies that considered UBI_{29-41} as a targeting molecule against bacteria owing to the attraction between the mutual charges.[43,44]

Penetration of Bacterial Biofilms in vitro

Biofilms with 24-h-old *S. aureus* and MRSA were treated with 1 μg/mL of MXF or MXF@UiO-UBI-PEGTK. CLSM images of live/dead bacterial staining revealed that MXF killed only *S. aureus* and MRSA at the surface of the biofilm, and an addition of 0.25 mM H_2O_2 had no significant effects. MXF@UiO-UBI-PEGTK killed *S. aureus* and MRSA beyond the surface, and the addition of H_2O_2 (0.25 mM) significantly increased biofilm penetration and antibacterial effect up to a depth of 9 μm (Figure 4). Statistical analyses showed that MXF@UiO-UBI-PEGTK with 0.25 mM H_2O_2 killed more bacteria than other groups (MXF, MXF + 0.25 mM H_2O_2; MXF@UiO-UBI-PEGTK) at the same depth (all $p < 0.05$) (Tables S1 and S2). Considering the biofilm of *S. aureus*, the mortality rate of bacteria in the MXF group was close to zero when the depth of biofilm reached 6 μm, in which only 0.57% of the bacteria were killed. However, in the MXF@UiO-UBI-PEGTK group, 49.80% and 13.08% of the bacteria were killed at the same depth with or without 0.25 mM H_2O_2, respectively. Similarly, for the biofilm of MRSA, the antibacterial effect of MXF decreased and reached a plateau stage when the depth of biofilm reached 4 μm, wherein only 5.41% of the bacteria were killed. However, in the MXF@UiO-UBI-PEGTK group, 27.80% and 19.71% of the bacteria were killed at the same depth with or without 0.25 mM H_2O_2, respectively.

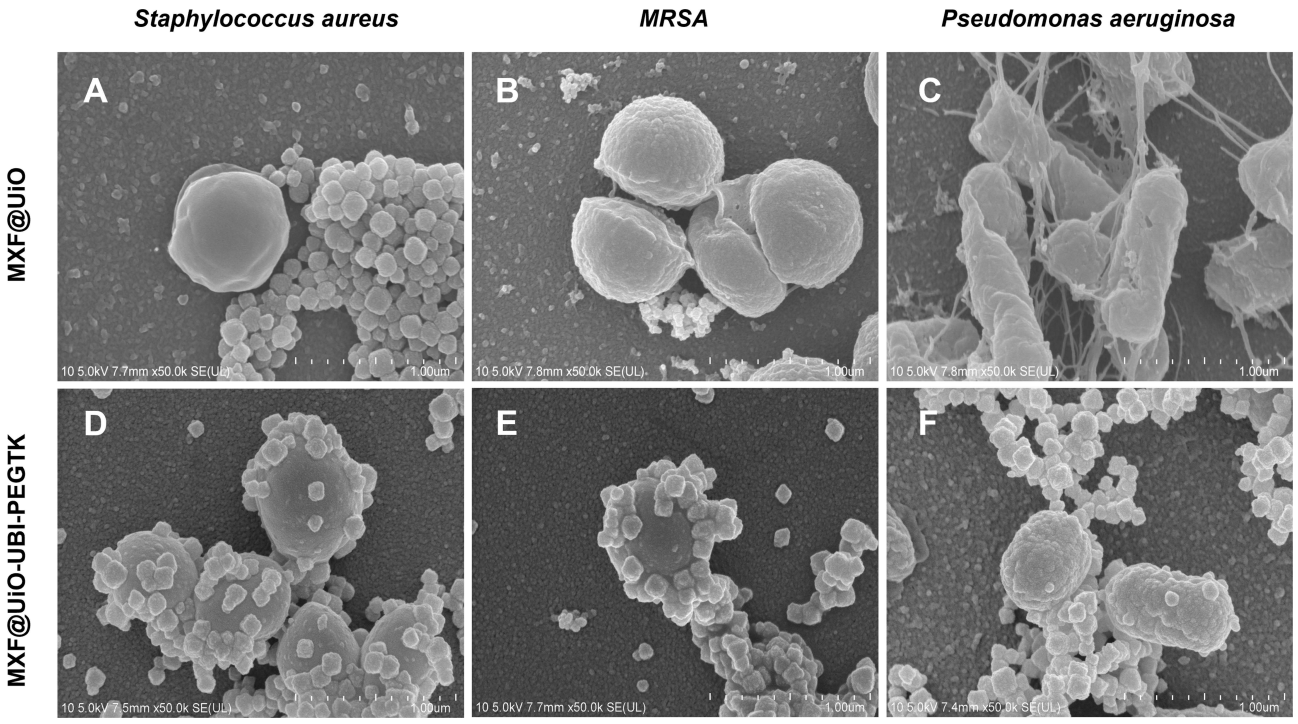

Figure 3 SEM images showing the targeting effect of (**A**–**C**) MXF@UiO and (**D**–**F**) MXF@UiO-UBI-PEGTK toward *S. aureus*, MRSA, and *P. aeruginosa*. Scale bar: 1 μm.

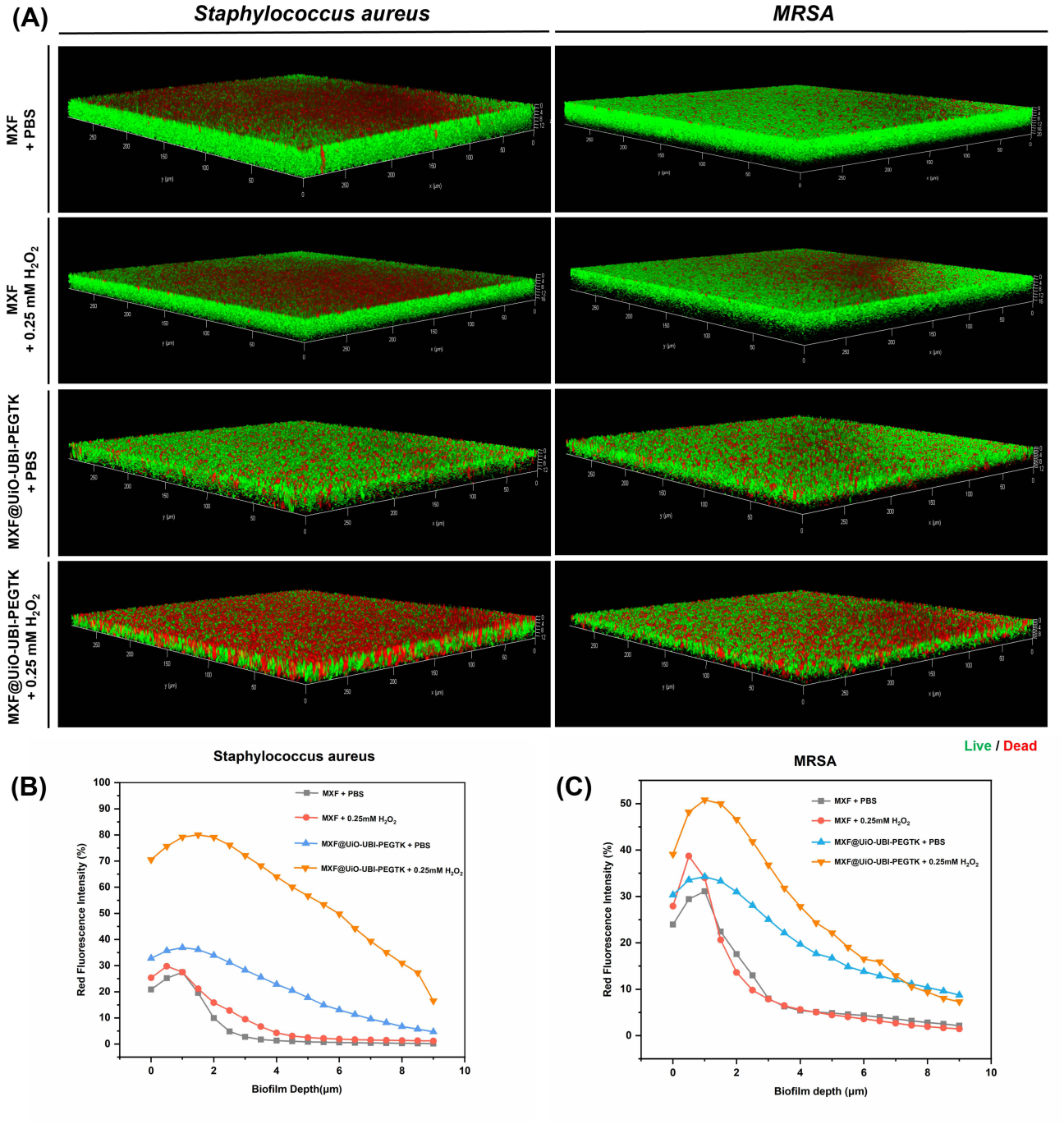

Figure 4 Penetration of bacterial biofilm in vitro. (**A**) Three-dimensional CLSM images of calcein/PI-stained *S. aureus*/MRSA biofilms treated with MXF or MXF@UiO-UBI-PEGTK with or without 0.25 mM H_2O_2, respectively. Red fluorescence intensity reflected the number of dead bacteria at different depths of (**B**) *S. aureus* and (**C**) MRSA biofilms in the above images (**A**).

Eradication of Bacterial Biofilms in vitro

To further evaluate their effect on bacterial biofilm eradication, the bacterial live/dead immunofluorescence staining and the flat counting methods were used to distinguish the remaining living bacteria in the biofilm. Using the bacterial live/dead staining method, a significant reduction in green fluorescence intensity (living bacteria) was observed in the biofilms treated with MXF@UiO-UBI-PEGTK and 0.25 mM H_2O_2 when compared with the other groups (Figure 5A). These results were confirmed using the flat counting method, as shown in Figure 5B. For all three bacterial biofilms, the number of CFUs in the MXF@UiO-UBI-PEGTK + 0.25 mM

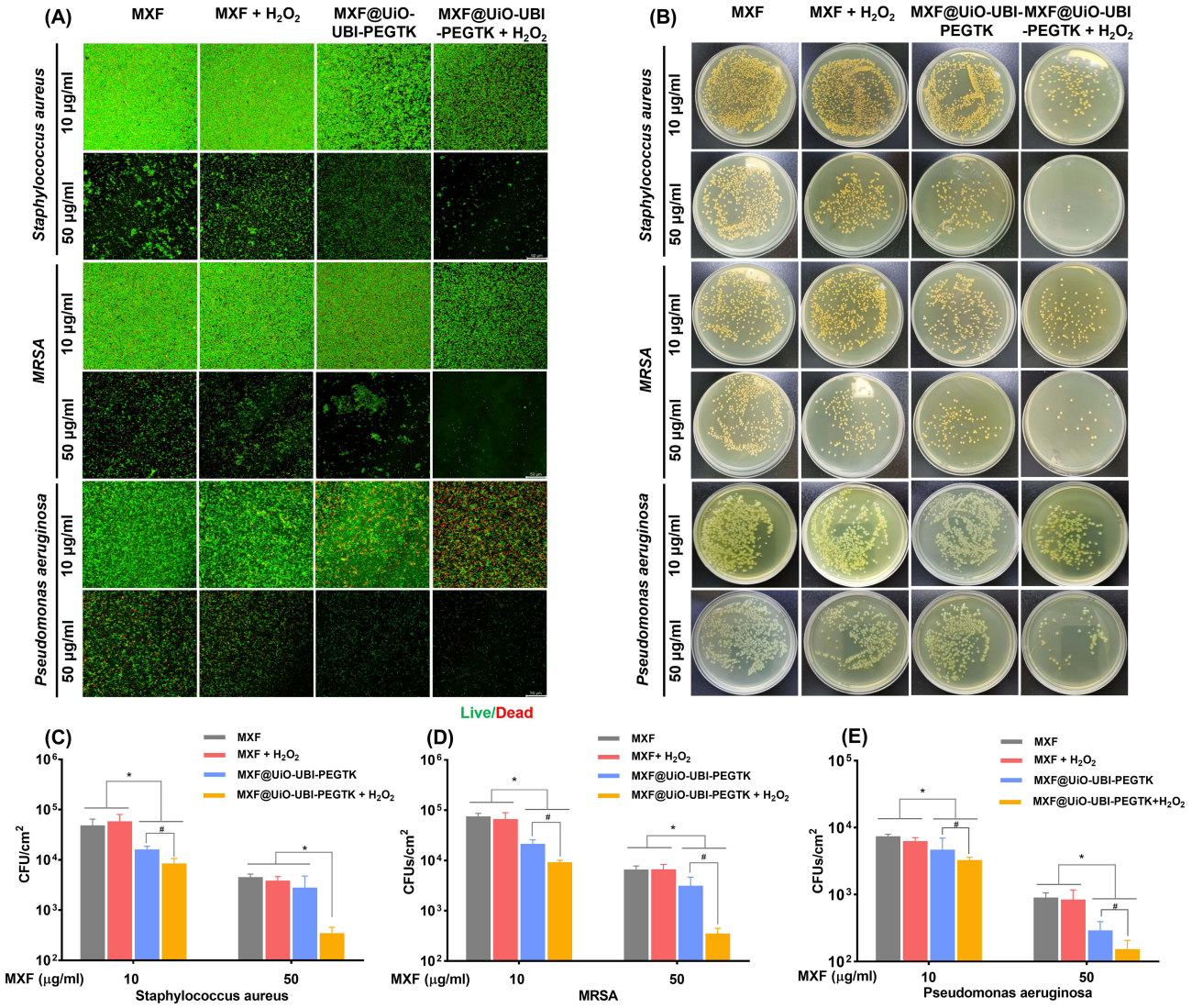

Figure 5 Eradication of bacterial biofilms in vitro. (**A**) Calcein/PI-stained images represented the live/dead bacteria on the *S. aureus* biofilm, MRSA biofilm and *P. aeruginosa* biofilm. Scale bar: 5 μm. (**B**) Photographs of the agar plates of *S. aureus*, MRSA, and *P. aeruginosa* colonies in corresponding biofilms after treatments with PBS, MXF, or MXF@UiO-UBI-PEGTK, respectively. (**C**–**E**) Quantitative analysis of CFUs in the corresponding agar plates in the above figure (**B**) (**p*, $^{\#}p < 0.05$) (**p*, MXF vs MXF@UiO-UBI-PEGTK or MXF + H_2O_2 vs MXF@UiO-UBI-PEGTK + H_2O_2; $^{\#}p$, MXF@UiO-UBI-PEGTK vs MXF@UiO-UBI-PEGTK + H_2O_2).

H_2O_2 group was the lowest among all four groups (all $p < 0.05$) (Figure 5C–E). These results indicated that MXF@UiO-UBI-PEGTK showed a stronger biofilm eradication effect than MXF, particularly with the addition of H_2O_2. To further verify the biofilm removal efficiency, SEM images were analyzed. The MXF@UiO-UBI-PEGTK + 0.25 mM H_2O_2 group showed excellent biofilm eradication efficacy as the bacteria adhering to the surface were significantly reduced (Figure 6).

These results indicated the excellent biofilm penetration and eradication effects of MXF@UiO-UBI-PEGTK and confirmed the desired properties of MXF@UiO-UBI-PEGTK. The effective ROS-responsive moieties (PEGTK) of MXF@UiO-UBI-PEGTK will decompose into acetone and thiol moieties when triggered by high levels of ROS (eg, H_2O_2, OH.) generated by inflammation. Subsequently, via the attractive interaction between the positively charged domain of $UBI_{29\text{-}41}$ and the negatively charged surface of the bacteria, the NPs, as well as the released MXF, accumulated at the bacterial infection sites. Besides our nanoparticle, two-tailed antimicrobial amphiphiles were reported to eradicate biofilms with excellent efficacy, which may be another option to load antibiotics.[23]

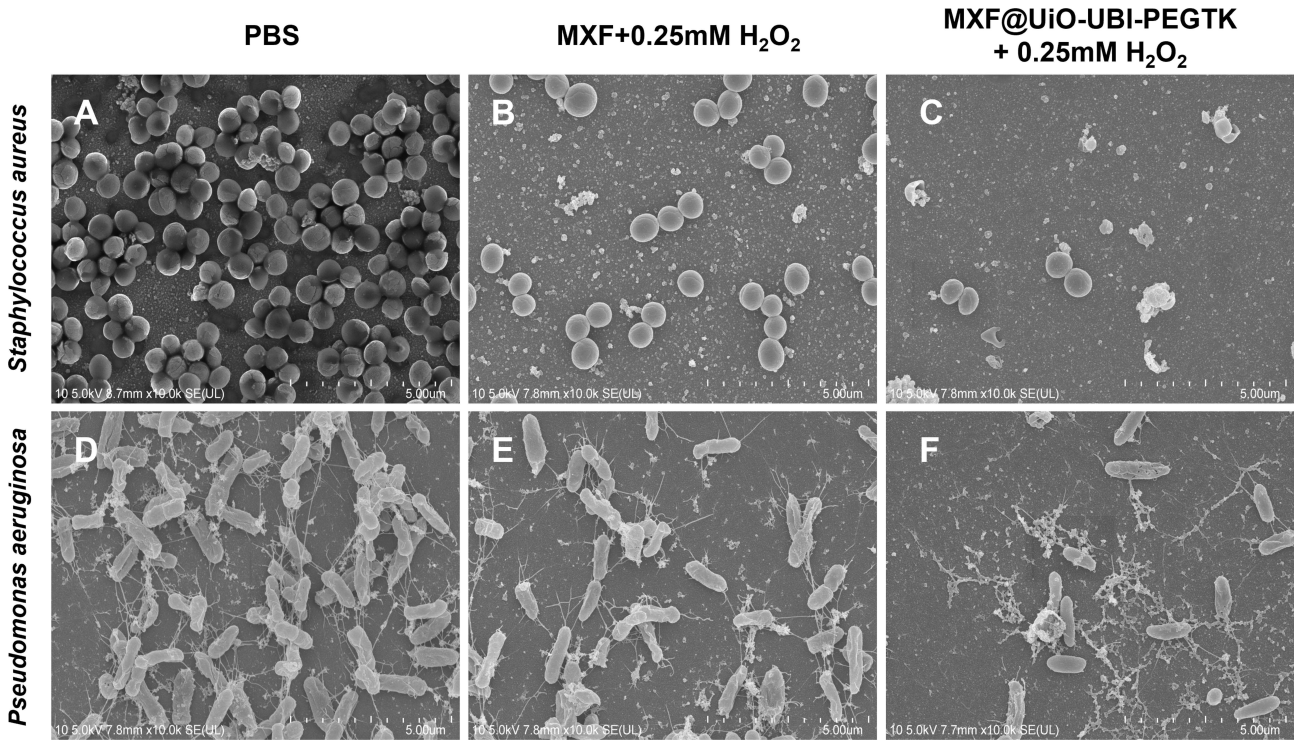

Figure 6 SEM images showing the antibiofilm properties of MXF and MXF@UiO-UBI-PEGTK with 0.25mM H_2O_2 against (**A**–**C**) S. aureus and (**D**–**E**) *P. aeruginosa*, respectively. Scale bar: 5 μm.

In vivo Antibacterial Tests

A bacterial endophthalmitis model was successfully constructed in New Zealand White rabbits through the intraocular injection of three types of bacterial solutions (*S. aureus*, MRSA, and *P. aeruginosa*). One day after injection, in the blank control group, the cornea and conjunctiva were clear, and no glint or exudation was observed in the anterior chamber, while anterior chamber empyema, conjunctival hyperemia, and purulent secretion were observed in the model groups. The eyes were treated with PBS, MXF, or MXF@UiO-UBI-PEGTK. In the endophthalmitis model of all three bacteria, in the eyes treated with MXF and MXF@UiO-UBI-PEGTK, secretions, bulbar conjunctival hyperemia, corneal edema, and anterior chamber inflammation were alleviated during the first 7 days after treatment. The signs and degree of inflammation in the MXF- and MXF@UiO-UBI-PEGTK-treated eyes were significantly milder than those in the PBS group (all $p < 0.05$). At the 10^{th} day, the inflammation degree scores were the lowest in the MXF@UiO-UBI-PEGTK-treated group (all $p < 0.05$), compared to the PBS and MXF groups (Figure 7).

At the 10^{th} day, the rabbits were euthanized, the eyeball was removed for further examination, and the vitreous humor was cultured on an agar plate for the flat counting of bacteria. Results showed that the number of CFUs of the three types of bacteria in the MXF@UiO-UBI-PEGTK-treated eyes (*S. aureus*: 5.2×10^2 CFUs, MRSA: 6.0×10^2 CFUs, and *P. aeruginosa*: 1.5×10^3 CFUs,) were lower than that in the MXF-treated group (*S. aureus*: 3.2×10^3 CFUs, MRSA: 2.0×10^4 CFUs, and *P. aeruginosa*: 1.0×10^4 CFUs,) (all $p < 0.05$). Hematoxylin and eosin (H&E) staining also indicated that the retina from the PBS- and MXF-treated eyes was almost destroyed, and the infiltration of inflammatory cells was severe (PBS: 54 ± 23 cells/HP; MXF: 15 ± 12 cells/HP), while the retinal structure from MXF@UiO-UBI-PEGTK-treated eyes was intact; the infiltration of inflammatory cells was mild (8 ± 3 cells/HP) and was significantly less than that of the PBS- and MXF-treated eyes (all $p < 0.05$) (Figure 8).

The in vivo antibacterial study confirmed the good antibacterial effect of MXF@UiO-UBI-PEGTK. The ROS-responsive release and targeting properties of the novel NPs, together with MXF, worked synergistically and

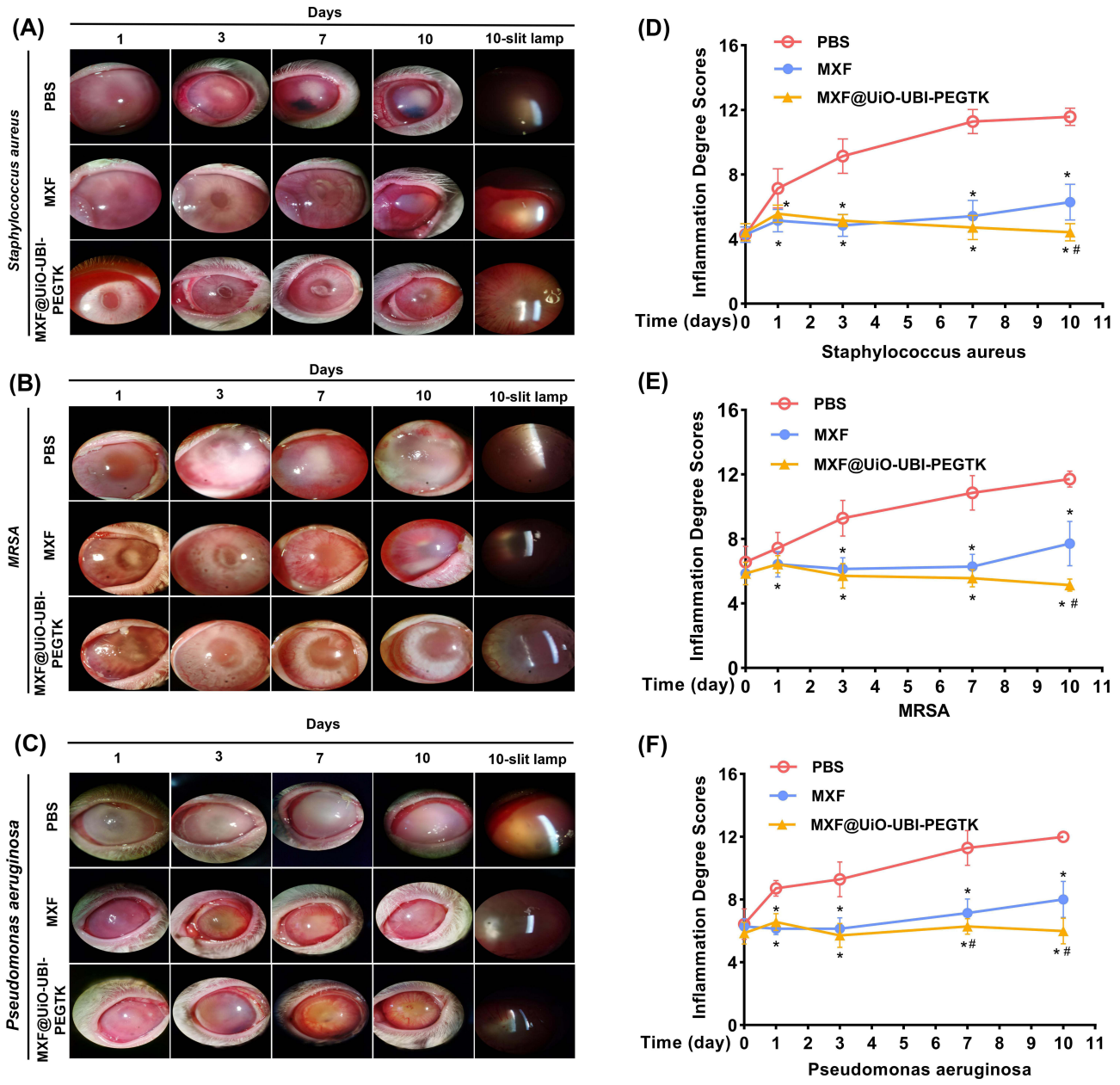

Figure 7 Evaluation of the antibacterial effects in vivo. Diffuse and slit lamp micrographs as well as the inflammation degree in corresponding endophthalmitis induced by (**A** and **D**) *S. aureus*, (**B** and **E**) MRSA, and (**C** and **F**) *P. aeruginosa* upon treatment with PBS, MXF, and MXF@UiO-UBI-PEGTK for 1, 3, 7, and 10 d, respectively (*p, $^{\#}p$ < 0.05) (*p, MXF or MXF@UiO-UBI-PEGTK vs PBS; $^{\#}p$, MXF vs MXF@UiO-UBI-PEGTK).

successfully against the infection. Besides, the excretion pathway of nanoparticles used in vivo is a major concern. Given the well-characterized and established hydrophilic nature of UiO-66, it is postulated that the primary excretion pathway in the eye is likely to follow the conventional route of aqueous humor drainage through a series of anatomical structures, including the trabecular meshwork, Schlemm's canal, collector channels, and the episcleral venous system, ultimately converging into the circulation system. Secondly, it has been reported that the UiO-66 material can enter the bloodstream and subsequently reach both the renal and digestive systems, including organs such as the liver, stomach, and small intestine, from which it is excreted through urine or feces. Notably, no adverse effects on liver or kidney function were observed during the excretion process, suggesting the biological safety of the UiO-66 nanomaterial system.[45]

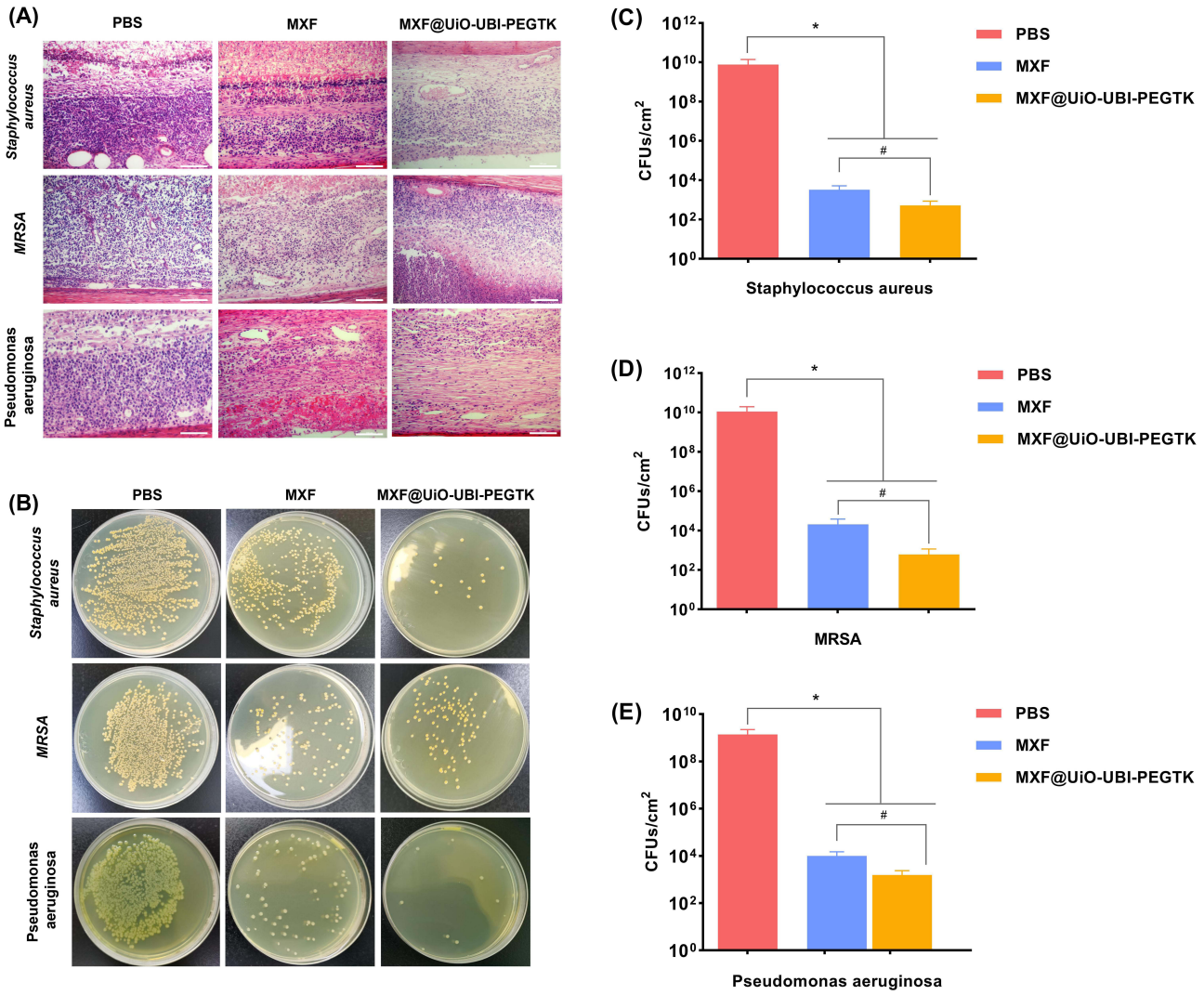

Figure 8 Histopathological evaluation of the antibacterial effects on endophthalmitis. (**A**) HE-staining photographs of the retinal tissues in endophthalmitis induced by *S. aureus*, MRSA, and *P. aeruginosa* treated with PBS, MXF, or MXF@UiO-UBI-PEGTK, respectively. Scale bar: 100 μm. (**B**) Photographs of the agar plates of *S. aureus*, MRSA, and *P. aeruginosa* colonies in vitreous fluid after treatments with PBS, MXF, or MXF@UiO-UBI-PEGTK, respectively. (**C**–**E**) Quantitative analysis of CFUs in the corresponding agar plates in the above figure (**B**) (*p, $^{\#}p < 0.05$) (*p, MXF or MXF@UiO-UBI-PEGTK vs PBS; $^{\#}p$, MXF vs MXF@UiO-UBI-PEGTK).

Conclusions

Bacterial endophthalmitis is one of the most devastating diseases that leads to eye blindness. Biofilm formation is a critical issue in the therapy of endophthalmitis because it prevents the antibiotics from reaching microorganisms. NPs have been explored for the delivery of antibiotics in the treatment of endophthalmitis. In this study, we successfully developed MXF-loaded UiO-66 NPs harboring the bacteria-targeting peptide $UBI_{29\text{-}41}$ and coated them with ROS-responsive PEG-TK. The coating of PEG-TK outside the NPs acted as a gate that prevented drug release until the particles reached the infectious tissue with a high level of ROS; therefore, the site-specific release of the drug could be achieved. The $UBI_{29\text{-}41}$ provided bacteria-targeting properties to the NPs. In vitro, MXF@UiO-UBI-PEGTK showed significant antibiotic effects as well as excellent biofilm penetration and eradication properties against *S. aureus, P. aeruginosa*, and MRSA under high ROS conditions. In vivo, MXF@UiO-UBI-PEGTK demonstrated outstanding efficacy in treating bacterial endophthalmitis. This novel NP system with ROS-responsive and bacteria-targeted properties promotes the precise and effective release of drugs and has significant potential for clinical application.

Data Sharing Statement

Data will be made available on request.

Acknowledgments

Jian Yu and Huan Xu are co-first authors for this study. This study was supported by research grants from the National Natural Science Foundation of China (Grant/Award Numbers: 82070980, 82201226, 82101087).

Disclosure

The authors report no conflicts of interest in this work.

References

1. Miller FC, Coburn PS, Huzzatul MM, LaGrow AL, Livingston E, Callegan MC. Targets of immunomodulation in bacterial endophthalmitis. *Prog Retinal Eye Res*. 2019;73:100763. doi:10.1016/j.preteyeres.2019.05.004
2. Durand ML. Bacterial and fungal endophthalmitis. *Clin Microbiol Rev*. 2017;30(3):597–613. doi:10.1128/CMR.00113-16
3. Brockhaus L, Goldblum D, Eggenschwiler L, Zimmerli S, Marzolini C. Revisiting systemic treatment of bacterial endophthalmitis: a review of intravitreal penetration of systemic antibiotics. *Clin Microbiol Infect*. 2019;25(11):1364–1369. doi:10.1016/j.cmi.2019.01.017
4. Lodha D, Karolia R, Sharma S, Joseph J, Das T, Dave VP. Biofilm formation and its effect on the management of culture-positive bacterial endophthalmitis. *Indian J Ophthalmol*. 2022;70(2):472–476. doi:10.4103/ijo.IJO_1872_21
5. Holland EJ, McDonald MB, Parekh JG, Sheppard JD. Antibiotic resistance in acute postoperative endophthalmitis. *Ophthalmology*. 2014;121(11): S1–9; quiz S10–12. doi:10.1016/j.ophtha.2014.06.049
6. Bispo P, Haas W, Gilmore M. Biofilms in Infections of the Eye. *Pathogens*. 2015;4(1):111–136. doi:10.3390/pathogens4010111
7. Stewart PS, Costerton JW. Antibiotic resistance of bacteria in biofilms. *Lancet*. 2001;358(9276):135–138. doi:10.1016/s0140-6736(01)05321-1
8. Hu D, Li H, Wang B, et al. Surface-adaptive gold nanoparticles with effective adherence and enhanced photothermal ablation of methicillin-resistant staphylococcus aureus biofilm. *ACS Nano*. 2017;11(9):9330–9339. doi:10.1021/acsnano.7b04731
9. Liu Y, Shi L, Su L, et al. Nanotechnology-based antimicrobials and delivery systems for biofilm-infection control. *Chem Soc Rev*. 2019;48 (2):428–446. doi:10.1039/c7cs00807d
10. Wang Y, Jin Y, Chen W, et al. Construction of nanomaterials with targeting phototherapy properties to inhibit resistant bacteria and biofilm infections. *Chem Eng J*. 2019;358:74–90. doi:10.1016/j.cej.2018.10.002
11. Nasrabadi M, Ghasemzadeh MA, Zand Monfared MR. The preparation and characterization of UiO-66 metal–organic frameworks for the delivery of the drug ciprofloxacin and an evaluation of their antibacterial activities. *New J Chem*. 2019;43(40):16033–16040. doi:10.1039/C9NJ03216A
12. Bowen RC, Zhou AX, Bondalapati S, et al. Comparative analysis of the safety and efficacy of intracameral cefuroxime, moxifloxacin and vancomycin at the end of cataract surgery: a meta-analysis. *Br J Ophthalmol*. 2018;102(9):1268–1276. doi:10.1136/bjophthalmol-2017-311051
13. Chen H, Yang J, Sun L, et al. Synergistic chemotherapy and photodynamic therapy of endophthalmitis mediated by zeolitic imidazolate framework-based drug delivery systems. *Small*. 2019;15(47):1903880. doi:10.1002/smll.201903880
14. Zhang W, Liang L, Yuan X, et al. Intelligent dual responsive modified ZIF-8 nanoparticles for diagnosis and treatment of osteoarthritis. *Mater Des*. 2021;209:109964. doi:10.1016/j.matdes.2021.109964
15. Su L, Li Y, Liu Y. Antifungal-inbuilt metal–organic-frameworks eradicate *candida albicans* biofilms. *Adv Funct Mater*. 2020;30(28):2000537. doi:10.1002/adfm.202000537
16. Lollar CT, Qin J-S, Pang J, Yuan S, Becker B, Zhou H-C. Interior decoration of stable metal–organic frameworks. *Langmuir*. 2018;34 (46):13795–13807. doi:10.1021/acs.langmuir.8b00823
17. Li P, Vermeulen NA, Gong X, et al. Design and synthesis of a water-stable anionic uranium-based Metal-Organic Framework (MOF) with ultra large pores. *Angew Chem Int Ed*. 2016;55(35):10358–10362. doi:10.1002/anie.201605547
18. Kandiah M, Nilsen MH, Usseglio S. Synthesis and stability of tagged UiO-66 Zr-MOFs. *Chem Mater*. 2010;22(24):6632–6640. doi:10.1021/cm102601v
19. He L, Brasino M, Mao C, et al. DNA-assembled core-satellite upconverting-metal–organic framework nanoparticle superstructures for efficient photodynamic therapy. *Small*. 2017;13(24):1700504. doi:10.1002/smll.201700504
20. Cavka JH, Jakobsen S, Olsbye U, et al. A new zirconium inorganic building brick forming metal organic frameworks with exceptional stability. *J Am Chem Soc*. 2008;130(42):13850–13851. doi:10.1021/ja8057953
21. Mao J, Li Y, Wu T, et al. A simple dual-pH responsive prodrug-based polymeric micelles for drug delivery. *ACS Appl Mater Interfaces*. 2016;8 (27):17109–17117. doi:10.1021/acsami.6b04247
22. Zhan Y, Hu X, Li Y, et al. Antimicrobial hybrid amphiphile via dynamic covalent bonds enables bacterial biofilm dispersal and bacteria eradication. *Adv Funct Mater*. 2023;33(23):2214299. doi:10.1002/adfm.202214299
23. Hu X, Li Y, Piao Y. Two-tailed dynamic covalent amphiphile combats bacterial biofilms. *Adv Mater*. 2023;35(33):e2301623. doi:10.1002/adma.202301623
24. Shi Y, van Steenbergen MJ, Teunissen EA, et al. Π–Π stacking increases the stability and loading capacity of thermosensitive polymeric micelles for chemotherapeutic drugs. *Biomacromolecules*. 2013;14(6):1826–1837. doi:10.1021/bm400234c
25. Nguyen MM, Carlini AS, Chien M-P, et al. Enzyme-responsive nanoparticles for targeted accumulation and prolonged retention in heart tissue after myocardial infarction. *Adv Mater*. 2015;27(37):5547–5552. doi:10.1002/adma.201502003
26. Chen L, Peng M, Zhou J, et al. Supramolecular photothermal cascade nano-reactor enables photothermal effect, cascade reaction, and in situ hydrogelation for biofilm-associated tooth-extraction wound healing. *Adv Mater*. 2023;35(31):e2301664. doi:10.1002/adma.202301664
27. Mura S, Nicolas J, Couvreur P. Stimuli-responsive nanocarriers for drug delivery. *Nat Mater*. 2013;12(11):991–1003. doi:10.1038/nmat3776

28. Mittal M, Siddiqui MR, Tran K, Reddy SP, Malik AB. Reactive oxygen species in inflammation and tissue injury. *Antioxid. Redox Signaling*. 2014;20(7):1126–1167. doi:10.1089/ars.2012.5149
29. Kim Y, Uthaman S, Pillarisetti S, Noh K, Huh KM, Park I-K. Bioactivatable reactive oxygen species-sensitive nanoparticulate system for chemo-photodynamic therapy. *Acta Biomater*. 2020;108:273–284. doi:10.1016/j.actbio.2020.03.027
30. Jin F, Qi J, Liu D, et al. Cancer-cell-biomimetic upconversion nanoparticles combining chemo-photodynamic therapy and CD73 blockade for metastatic triple-negative breast cancer. *J Control Release*. 2021;337:90–104. doi:10.1016/j.jconrel.2021.07.021
31. Zhao Y, Xie R, Yodsanit N, Ye M, Wang Y, Gong S. Biomimetic fibrin-targeted and H2O2-responsive nanocarriers for thrombus therapy. *Nano Today*. 2020;35:100986. doi:10.1016/j.nantod.2020.100986
32. Zhu Y, Yao Z, Liu Y, Zhang W, Geng L, Ni T. Incorporation of ROS-responsive substance P-loaded zeolite imidazolate framework-8 nanoparticles into a Ca2+-cross-linked alginate/pectin hydrogel for wound dressing applications. *Int J Nanomed*. 2020;15:333–346. doi:10.2147/IJN.S225197
33. Pei P, Sun C, Tao W, Li J, Yang X, Wang J. ROS-sensitive thioketal-linked polyphosphoester-doxorubicin conjugate for precise phototriggered locoregional chemotherapy. *Biomaterials*. 2019;188:74–82. doi:10.1016/j.biomaterials.2018.10.010
34. Ling X, Zhang S, Shao P, Wang P, Ma X, Bai M. Synthesis of a reactive oxygen species responsive heterobifunctional thioketal linker. *Tetrahedron Lett*. 2015;56(37):5242–5244. doi:10.1016/j.tetlet.2015.07.059
35. Li J, Ding Z, Li Y. Reactive oxygen species-sensitive thioketal-linked mesoporous silica nanoparticles as drug carrier for effective antibacterial activity. *Mater Des*. 2020;195:109021. doi:10.1016/j.matdes.2020.109021
36. Chung PY, Khanum R. Antimicrobial peptides as potential anti-biofilm agents against multidrug-resistant bacteria. *J Microbiol Immunol Infect*. 2017;50(4):405–410. doi:10.1016/j.jmii.2016.12.005
37. Singh R, Prasad A, Kumar B, Kumari S, Sahu RK, Hedau ST. Hedau, potential of dual drug delivery systems: MOF as hybrid nanocarrier for dual drug delivery in cancer treatment. *ChemistrySelect*. 2022;7(36):e202201288. doi:10.1002/slct.202201288
38. Chansi, Upreti S, Punya, Singh J, Ghosh MP, Basu T. Rapid electrochemical quantification for in vitro release trait of ophthalmic drug loaded within Mucoadhesive Metal Organic Framework (MOF). *ChemistrySelect*. 2021;6(12):3006–3012. doi:10.1002/slct.202004558
39. Ung L, Pattamatta U, Carnt N, Wilkinson-Berka JL, Liew G, White AR. Oxidative stress and reactive oxygen species: a review of their role in ocular disease. *Clin Sci*. 2017;131(24):2865–2883. doi:10.1042/CS20171246
40. Singh PK, Kumar A, Kumar A. Molecular mechanisms of retinal cell death in Staphylococcus aureus endophthalmitis. *Invest Ophthalmol Visual Sci*. 2015;56:872.
41. Mursalin MH, Coburn PS, Miller FC, Livingston ET, Astley R, Callegan MC. Innate immune interference attenuates inflammation in bacillus endophthalmitis. *Invest Opthalmol Visual Sci*. 2020;61(13):17. doi:10.1167/iovs.61.13.17
42. Miyake H, Miyazaki D, Shimizu Y, et al. Toxicities of and inflammatory responses to moxifloxacin, cefuroxime, and vancomycin on retinal vascular cells. *Sci Rep*. 2019;9(1):9745. doi:10.1038/s41598-019-46236-2
43. Saeed S, Zafar J, Khan B, et al. Utility of ^{99}mTc-labelled antimicrobial peptide ubiquicidin (29-41) in the diagnosis of diabetic foot infection. *Eur J Nucl Med Mol Imag*. 2013;40(5):737–743. doi:10.1007/s00259-012-2327-1
44. Yang S, Han X, Yang Y, et al. Bacteria-targeting nanoparticles with microenvironment-responsive antibiotic release to eliminate intracellular staphylococcus aureus and associated infection. *ACS Appl Mater Interfaces*. 2018;10(17):14299–14311. doi:10.1021/acsami.7b15678
45. Jarai BM, Stillman Z, Attia L, Decker GE, Bloch ED, Fromen CA. Evaluating UiO-66 metal–organic framework nanoparticles as acid-sensitive carriers for pulmonary drug delivery applications. *ACS Appl Mater Interfaces*. 2020;12(35):38989–39004. doi:10.1021/acsami.0c10900